Atomic-scale Monte Carlo study of step-flow growth modes on GaAs(001)-(2×4)

Makoto Itoh* and Takahisa Ohno
National Research Institute for Metals, 1-2-1 Sengen, Tsukuba, Ibaraki 305-0047, Japan
(Received 8 June 2000; revised manuscript received 8 September 2000; published 1 March 2001)

The step-flow growth modes of the GaAs(001)-$\beta 2(2\times4)$ structure growing by molecular-beam homoepitaxy are studied by the Monte Carlo simulation method using a two-species kinetic growth model. Our results show that a terrace edge parallel to the $[\bar{1}10]$ direction does not grow in a coherent manner but by the growth of rather short segments of As dimer rows. For terrace edges perpendicular to this direction, we find that the growth morphology depends strongly on the relative phase of the (2×4) structure between an upper terrace and a lower one. More precisely, when they are out of phase with each other in the [110] direction, growth proceeds principally by kink propagation in this direction, whereas, if they are in phase with each other, an As dimer row grows on top of the As dimer rows of the lower terrace, followed by growth in the directions perpendicular to it, resulting in the creation of a peninsula.

DOI: 10.1103/PhysRevB.63.125301 PACS number(s): 68.55.−a, 68.03.Fg, 68.35.Fx, 02.70.Rr

I. INTRODUCTION

Recently, the important role of surface reconstruction has been increasingly realized not only in crystal growth but also in the development of optoelectronic devices.[1–22] To develop such devices, extensive use has been made of III-V compound semiconductors, among which the GaAs(001)-$\beta 2(2\times4)$ structure is the best known surface reconstruction.[23] To monitor its growth in molecular-beam epitaxy (MBE),[24] the oscillation phenomenon[25] of the specular intensity I_s in reflection high-energy electron diffraction (RHEED) is often used because of its geometrical advantage.[26] Studying the time evolution of this intensity, Neave *et al.* found the disappearance of this oscillation when the substrate temperature was increased.[27] They interpreted this phenomenon as a growth mode transition between an island growth mode at low temperature and a step-flow growth mode at high temperature, noting that the diffusion length of adatoms is enhanced by an increase of temperature, so that these atoms can reach a nearby step edge more easily at high temperature.[27]

Following this study, Shitara *et al.* carried out kinetic Monte Carlo (KMC) simulations[28–30] by using the one-species solid-on-solid (SOS) model and compared the observed I_s with the simulated step densities at various growth conditions.[31–33] They first compared the growth mode transition in simulations and experiments on surfaces tilted from the [001] direction toward the [010] direction (*C* surfaces), and obtained the effective diffusion barrier $E_s=1.58\pm0.02$ eV for the MBE growth conditions in which the (2×4) structure is maintained.[31,32] In these studies, they selected the *C* surfaces so as to reduce the effect of anisotropy in the growth kinetics. By using RHEED, they further observed the growth mode transition on the *A* and *B* surfaces, which are tilted from the [001] direction toward the [110] and the $[\bar{1}10]$ direction, respectively, and found that the transition takes place at a higher temperature on the *A* surfaces than on the *B* surfaces for all growth conditions they examined.[33] By comparing these results with simulations, they concluded that the sticking coefficient in the SOS model is larger in the $[\bar{1}10]$ direction (*B* step) than in the [010] direction (*A* step).

However, we must point out that they succeeded in obtaining $E_s=1.58\pm0.02$ eV because the growth mode transition is rather insensitive to the atomic-scale growth kinetics on a *C* surface only. Moreover, one must pay attention to the fact that the (2×4) structure, or, more precisely, the $\beta 2(2\times4)$ structure, is As terminated, as depicted in Fig. 1, whereas the principal diffusive species on it is Ga.[27,34] Even more importantly, there is a difference in the number of Ga adatoms necessary for step-flow grow to occur, as we will see in Figs. 3(a) and 3(b) below. Therefore, even if similar comparisons with simulations to those on the *C* surfaces[31,32] are made on *A* or *B* surfaces, one cannot correctly identify the origin of the difference in step-flow growth modes between them. In spite of these facts, Shitara *et al.* ascribed the difference in growth modes between them to anisotropy in the sticking coefficients of the constituent of the one-species SOS model.[33] However, this is an entirely model-dependent result, which has no generality. Indeed, there are some counterexamples, in which the diffusion around the corner of an island[35–37] or along a step[38,39] plays a crucial role in the anisotropic growth of epitaxial islands.

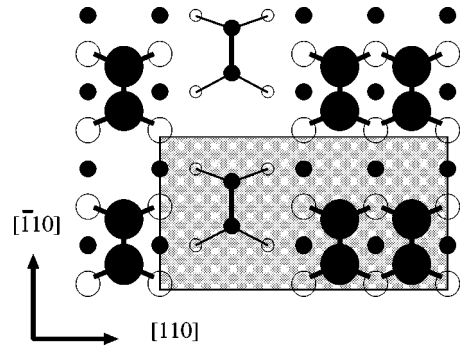

FIG. 1. Plan view of the $\beta 2(2\times4)$ structure with the crystallographic directions indicated by the arrows. The dark and bright disks represent As atoms and Ga atoms, respectively, and their radii decrease according to their depths.

Furthermore, since the SOS model is constructed on the simple cubic lattice, the simulated step density always increases upon starting growth, and decreases after its interruption, irrespective of the vicinal orientation of the surface. Therefore, if the simulated step density obtained by using the SOS model gives the correct account of the time evolution of I_s, it must evolve similarly on the surfaces of any vicinal orientations. However, we can see in Figs. 1–3 of Ref. 33 that I_s observed on *A* surfaces evolves completely differently from I_s on *B* or *C* surfaces. It is clear from this that the simulation part of Ref. 33 does not provide the correct account of its experimental part.

Thus we must use a more realistic model than the SOS model to study the step-flow growth modes of a GaAs(001)-$\beta 2(2\times4)$ reconstructed surface with different vicinal orientations. For this purpose, we use the two-species model[8–10] and carry out growth simulations of *A* and *B* steps as the first step toward a full and correct understanding of the step-flow growth modes on the vicinal surfaces of GaAs(001). This is a natural choice to this end since both Ga and As species play important roles in the atomic-scale growth kinetics of GaAs(001).[1–12,40–43]

A *C* step can of course be defined macroscopically as a surface on which the mean orientations of terrace edges are aligned in the $\langle 010\rangle$ directions. Microscopically, however, this definition has a very large variety, since these directions are not the symmetry axes of the $\beta 2(2\times4)$ unit cell, and hence we do not consider it here. Moreover, since the growth kinetics depends on the surface atomic structure,[1–12] we restrict ourselves to studying the step-flow growth of the GaAs(001)-$\beta 2(2\times4)$ reconstruction, which appears as the stable reconstruction in the temperature range $T=580\pm20\,^{\circ}\mathrm{C}$. Thus, we choose $T=580\,^{\circ}\mathrm{C}$ as the temperature of the substrate in our simulations.

This paper is organized as follows. In Sec. II, we report our simulation results of the step-flow growth modes of *A* and *B* surfaces at an atomic scale. In contrast to the conventional understanding, we find that an *A* surface does not grow coherently. Instead, it grows as rather short segments of As dimer rows. For a *B* surface, we find that of the phase difference in the $\beta 2(2\times4)$ structure between an upper terrace and a lower one plays a significant role in the morphology of the growing terrace edge. Since we have pointed out the failure of the SOS model to simulate the growth of an *A* surface, we need to show that our simulation results are consistent with RHEED experiments. This is done in Sec. III with some qualitative arguments. We discuss our results in Sec. IV. Section V is devoted to the conclusions.

II. GROWTH SIMULATION OF TERRACE EDGES

By using the two-species model, we simulate growth of *A* and *B* steps, or more precisely the terrace edges of the corresponding surfaces. This model has been used to simulate the nucleation and growth of islands on GaAs(001) and InAs(001) in homoepitaxy.[8–10] Only the interaction diagrams of the As part are shown in Figs. 2(a)–2(e), in which Figs. 2(a) and 2(b) are attractive, and the rest are all repulsive.[44] Among them, the interaction depicted in Fig. 2(d) causes the

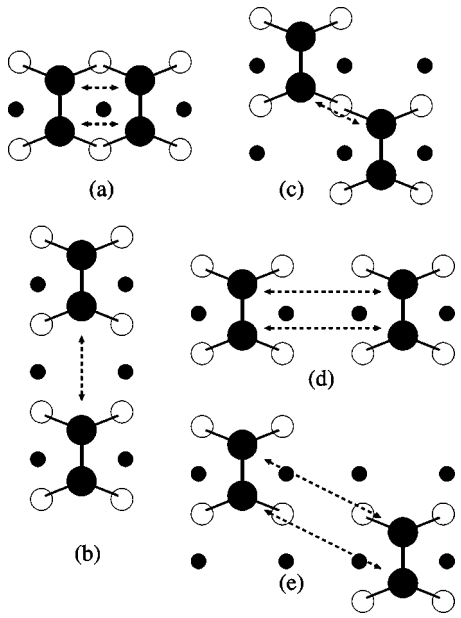

FIG. 2. As part of the interactions. The back bonding energy contribution to the activation barrier is 1.65 eV per atom, which is increased by the attractive interactions in (a) and (b) by (a) 1.00 eV and (b) 0.63 eV, and decreased by the repulsive ones in (c–e) by (c) 0.15 eV, (d) 1.21 eV, and (e) 0.25 eV.

structural transition of a growing island from a non-(2×4) structure to the $\beta 2(2\times4)$ structure.[8–10] Specifically, we use the same growth conditions as we used in the simulations of an island growth mode on GaAs(001), i.e., we set the substrate temperature to be $T=580\,^{\circ}\mathrm{C}$, and the Ga and As_2 fluxes to be 0.1 and 0.4 monolayers per second (ML/s), respectively. We chose these growth conditions partly because the $\beta 2(2\times4)$ reconstruction is stable at $T\simeq580\,^{\circ}\mathrm{C}$, as we stated above, and partly because the interaction parameters of the model were determined solely by comparing the simulation results with scanning tunneling microscope (STM) images[8–10] obtained by growth at this temperature. In these comparisons, special attention was paid to the aspect ratio of the growing two-dimensional (2D) islands between the directions parallel and perpendicular to the As dimer rows of the $\beta 2(2\times4)$ structure.[45]

Furthermore, we set the diffusion anisotropy of a Ga adatom g to be 3–5 times as large in the $[\bar{1}10]$ direction as in the $[110]$ direction when it is in the trench site of a well-ordered $\beta 2(2\times4)$ structure.[27,34] If this condition is not met, the diffusion anisotropy of a Ga adatom is reversed to be three times as large in the $[110]$ direction as in the $[\bar{1}10]$ direction. It is this change of the diffusion anisotropy that enables the occurrence of a structural transition from a non-(2×4) structure to the $\beta 2(2\times4)$ structure rather quickly.[8–10] Although we choose the anisotropy of the diffusion of a Ga adatom in the $[\bar{1}10]$ direction in the range between 3 and 5, this is because we carry out simulations on a finite size lattice, where a very large anisotropy merely results in a cycle of diffusion across the lattice. Accordingly, we find that the computation time increases as g is made larger. Fortunately, in practice, we find that simulation re-

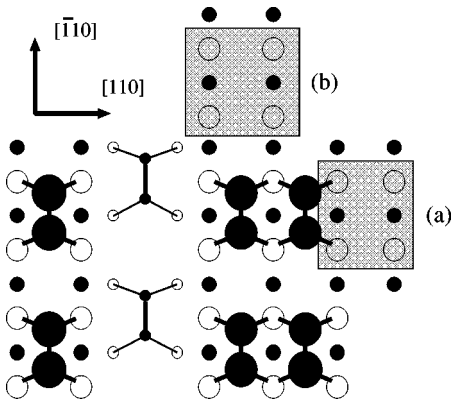

FIG. 3. In order to accommodate an As dimer, (a) an *A* step needs two Ga adatoms, but (b) a *B* step needs four of them, as the shaded areas indicate.

sults do not differ significantly when $3 \leqslant g < 10$, though we must keep in mind that g can have a much larger value than those we used in our simulations since the diffusion barrier of a Ga adatom is smaller in the $[\bar{1}10]$ direction than in the $[110]$ direction by about 0.3 eV on the $\beta 2(2\times4)$ structure in the absence of other adsorbate species.[34]

Here we note that, in principle, the same growth mechanism that was found to work in the island growth mode must work in the step-flow growth mode, too. This means further that we must not introduce any interactions specific to a terrace edge, because, at an atomic scale, there is no difference between the edges of an island and those of a terrace. This is particularly important in our simulation study since an Ehrlich-Schwoebel barrier[46–49] does not exist on the reconstructed GaAs(001)-$\beta 2(2\times4)$ surface.[12]

Before going into detail, we note two important properties in our simulations of the step-flow growth modes on GaAs(001). The first concerns the Ga kinetics, in which only two Ga adatoms are needed for the growth of an *A* step to begin, while four of them are required for a *B* step, as Figs. 3(a) and 3(b) clearly show. The second property is that, with the growth conditions stated above, we found nucleation and growth of islands to occur in all our simulations irrespective of the orientations of the steps. Obviously, this result disagrees with Shitara *et al.*'s experiments, in which no oscillation of specular RHEED intensity was observed on *B* surfaces at $T \simeq 580\,^{\circ}\mathrm{C}$.[33] We will discuss this problem later in Sec. IV.

Now we investigate the step-flow growth modes at an atomic scale. For this purpose, we first simulate growth of straight *A* steps, and next examine the effect of phase differences in the $\beta 2(2\times4)$ structures between an upper terrace and a lower one at various straight *B* steps. The growth simulations are carried out on a 2D lattice with periodic boundary conditions (PBC's). The lattice size $L\times L$ is chosen to be $200a_s \times 200a_s$ for the *A* steps in Sec. II A and $120a_s \times 120a_s$ for the *B* steps in Sec. II B, where $a_s = 4.0$ Å denotes the surface lattice constant of the GaAs(001) surface. We use a larger 2D lattice to simulate the growth of *A* steps because it is not easy for a Ga adatom to reach a straight *A* step for $g > 1$. Therefore, we need to use a large enough 2D lattice to allow sufficiently long diffusion of the Ga adatom. In contrast, no such need exists in simulating the growth of a *B* step since $g > 1$ means that a Ga adatom can easily arrive at it.

If we used multiterraces in the same way as did Shitara *et al.*[33] for the study of the step-flow growth modes, we should also use helical boundary conditions (HBC's) instead of PBC's because the model is constructed on the zinc-blende structure. However, the use of HBC's may result in the introduction of unexpected effects in the diffusion of Ga adatoms. Therefore, instead of using a set of stairs as well as the HBC's, we use a narrow strip of the terrace that is one bilayer higher than the substrate, place this strip across the central part of the substrate, and set its width to be $W = 10a_s$. Furthermore, all ends of the substrate and strip are connected by the PBC's whenever the ends reach the boundaries of the 2D lattice.

With this choice, the corresponding angle of misorientation of a vicinal surface is given by $\theta = \tan^{-1}[2d/(L-W)]$, where $d = 2.8$ Å is the bilayer height of the GaAs(001) surface. Hence, $\theta \approx 0.73°$ for $L = 120a_s$, which is used for the simulations of the *B* steps in Sec. II B, whereas θ takes an even smaller value for $L = 200a_s$ which is used in Sec. II A, as we noted before. Since these values of θ are smaller than the misorientation angles used in the RHEED observations of real GaAs(001) surfaces,[31–33] the sizes of the 2D lattices we used as the lower terraces are sufficiently large as to avoid artifacts caused by interstep interactions beyond the boundaries of the lattice, and to obtain reliable results from the simulations. As for the direct step-step interactions across a strip, we examined this effect by changing *W*, and found that the snapshots do not change significantly for $W \geqslant 10a_s$.

A. *A* steps

In this section, we simulate the growth of straight *A* steps, and, to this end, we use a narrow strip having straight *A* steps on both sides as the initial condition [see Fig. 4(a)]. We use a $200a_s \times 200a_s$ lattice and choose $g = 3$ for the diffusion anisotropy. Note that only the central parts of the snapshots are shown below.

In general, when a pair of Ga atoms arrives at the lower side of an *A* step via diffusion, an As_2 molecule may stick onto them and locally change the $\beta 2(2\times4)$ structure into the $\beta 1(2\times4)$ structure. When this process continues and the width of this structure exceeds the threshold for the structural transition from a non-(2×4) structure to the $\beta 2(2\times4)$ structure found in simulations of the island growth mode,[8–10] a similar transition occurs at the *A* step edge. More precisely, although an As dimer at the terrace edge of an *A* surface usually desorbs from there due to the Coulomb repulsion[50] corresponding to the interaction diagrams depicted in Figs. 2(d)–2(e), the splitting of a wide As dimer row may occur with a small but finite rate, as seen in Figs. 4(b)–4(d). Then, once it occurs, a wide As dimer row splits successively along itself when its width exceeds the threshold. However, since the diffusion anisotropy of Ga adatoms is enhanced in the $[\bar{1}10]$ direction, it is actually difficult for sufficiently many Ga adatoms to reach a straight *A* step in a short period of

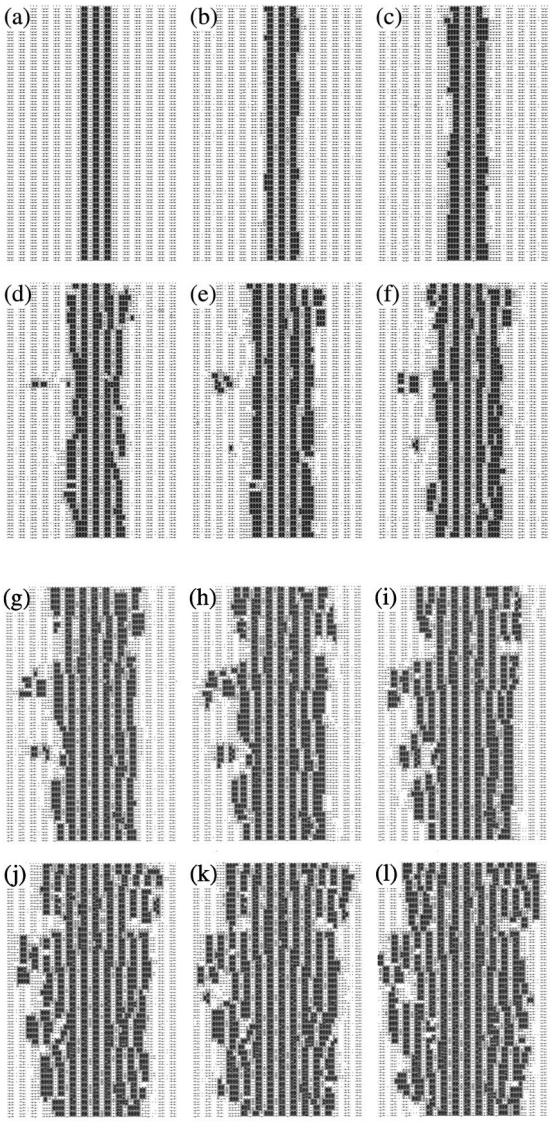

FIG. 4. A series of snapshots showing the simulated growth of a strip having straight *A* steps on both sides at every 0.5 s. These snapshots are taken from the central area of a $200a_s \times 200a_s$ lattice. Ga and As_2 fluxes are 0.1 ML/s and 0.4 ML/s, respectively, and $g=3$ is used for the diffusion anisotropy of the Ga adatom. (a) Initial configuration, i.e., the growth time $t=0.0$ s. A narrow strip is placed across a $200a_s \times 200a_s$ lattice at its central part. (b) $t=0.5$ s. The As dimer rows at the terrace edges become wide in short segments. (c) $t=1.0$ s. The As dimer rows become wider. (d) $t=1.5$ s. Wide As dimers are splitting in short segments. At the same time, an island has appeared on the left side. (e) $t=2.0$ s. The $\beta 2(2\times 4)$ structure is recovered inside the terrace. Another island has appeared in the bottom left side. (f) $t=2.5$ s. The process from (b) to (d) repeats. (g) $t=3.0$ s. The $\beta 2(2\times 4)$ structure is recovered inside the terrace again. (h) $t=3.5$ s. The islands on the left side are merged into the terrace edge. (i) $t=4.0$ s. (j) $t=4.5$ s. (k) $t=5.0$ s. (l) $t=5.5$ s. The terrace edges become less ordered on both sides.

time. Accordingly, this splitting phenomenon occurs randomly at various sites for short segments and, hence, the length of this local structure is found to be rather limited, up to about ten As dimers in the $[\bar{1}10]$ direction, as seen in Fig. 4(d). Later, these short segments merge together to construct rows of As dimers again, as seen in Fig. 4(e), where the $\beta 2(2\times 4)$ structure is recovered inside the terrace. Moreover, Figs. 4(e)–4(f) show that this process repeats itself as growth proceeds. At the same time, islands are found to nucleate even very close to an *A* step edge, as seen in the left side of Figs. 4(d) and 4(e). This is a consequence of the fact that the diffusion anisotropy of a Ga adatom is enhanced in the $[\bar{1}10]$ direction. At later stages, these islands coalesce with the growing terrace edge, as seen in Figs. 4(g)–4(k). In the last snapshot in Fig. 4(l), the terrace edges look rather disordered on both sides, in spite of the fact that coalescence between islands and a terrace occurred only on the left side of it and not on the right side.

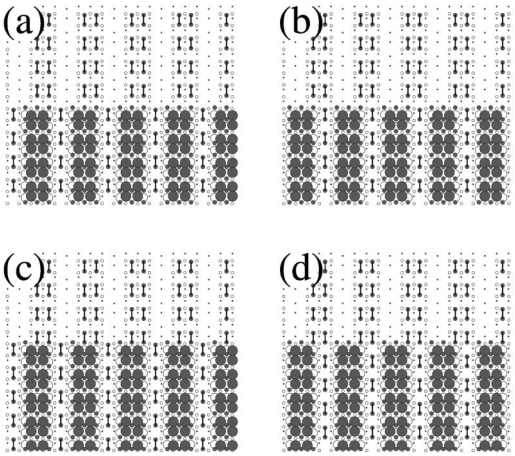

FIG. 5. Four possible phase differences in the $\beta 2(2\times 4)$ structures between an upper terrace and a lower one to make a *B* step. Two terraces are in phase with each other in the $[\bar{1}10]$ direction in (a) and (b), and in phase with each other in the $[110]$ direction in (a) and (c). We call the *B* steps in (a–d) *B*1, *B*2, *B*3, and *B*4, respectively.

B. *B* steps

Because of the periodicities of the $\beta 2(2\times 4)$ reconstruction, there are 16 principal patterns in the phase shifts of the $\beta 2(2\times 4)$ structure between an upper terrace and a lower one along a straight *B* step. This can be easily understood as follows. First, taking account of the mirror symmetry of the $\beta 2(2\times 4)$ structure in the $[110]$ direction, there are two possible phase shifts between two adjacent terraces in this direction according to the relative phases of the atomic structures between these terraces. Similarly, there are two possible phase shifts between these terraces in the $[\bar{1}10]$ direction. Furthermore, on each terrace, the phase difference between the As dimer rows on top of an As dimer hill of the $\beta 2(2\times 4)$ structure and those at a trench site can have two alternative possibilities. Thus, there are totally $2^4=16$ possible patterns in the phase difference at a *B* step edge. In this counting, for simplicity, we neglected possible unusual bonding of arsenic species near a terrace edge.

Among them, however, we consider the four principal cases shown in Figs. 5(a)–5(d). For a guide to the eyes, the

As dimer bonds in the trench sites of the upper terraces and those on the As dimer hills of the lower terraces are depicted in these figures by balls and sticks, which emphasize the phase differences in the As dimer rows between the two terraces. Although there are 12 other possibilities for the phase difference on a real surface, we do not consider them here since there is no difference in the model between the backbonding energies of a Ga adatom on the atop site of an As dimer and on the interdimer site of two As dimers adjacent to each other in the $[\bar{1}10]$ direction. Henceforth, we focus on the four types seen in Figs. 5(a)–5(d).

Between the possible directions of the phase shift in $[\bar{1}10]$ and $[110]$, let us first examine the shift in the $[110]$ direction. In this case, in order for the As dimer rows in the upper terraces of Figs. 5(b) and 5(d) to grow in the $[\bar{1}10]$ direction, the trenches in the lower terraces must be filled in first because the double As dimer rows in the upper terrace lie above the trenches of the lower terrace. In Figs. 5(a) and 5(c), in contrast, at least single As dimer rows can grow from the upper terraces in the $[\bar{1}10]$ direction without filling in the trenches of the lower terraces. Thus, it is anticipated that the terrace edges in Figs. 5(a) and 5(c) have higher step-flow growth rates than those in Figs. 5(b) and 5(d). Likewise, according as two adjacent terraces are in phase with each other, there may appear some kind of differences in the growth morphology among these four patterns.

In contrast, the distinction between Figs. 5(a) and 5(b) and 5(c) and 5(d) lies in the fact that, for the upper terraces in Figs. 5(c) and 5(d) to grow, the trenches adjacent to the terrace edge on the lower terrace side must be filled with new As_2 dimers out of phase with the double As dimer rows of the lower terraces. Since this process is inevitably associated with the repulsive interaction in Fig. 2(c) in addition to those in Figs. 2(d) and 2(e), the step-flow growth modes in Figs. 5(c) and 5(d) must be less efficient than those in Figs. 5(a) and 5(b).

Hereafter, we call the steps in Figs. 5(a)–5(d) $B1$, $B2$, $B3$, and $B4$, respectively. The simulations are carried out on $120a_s \times 120a_s$ lattices, on which narrow strips having the long axes in the $[110]$ direction are placed, and snapshots are recorded to study the growth of steps on such strips. As for the diffusion anisotropy, we use $g=5$ for these simulations.

First, we show the growth of a $B1$ step in Figs. 6(a)–6(d), which are a series of snapshots obtained by the growth simulation with Fig. 5(a) as the initial condition. We can see in Fig. 6(a) that Ga adatoms can easily reach the lower side of the terrace edge due to their diffusion anisotropy. Accordingly, since one of the As dimers of the double As dimer rows on the upper terrace resides on top of the As dimer rows of the lower terrace, this As dimer row can grow rather easily as a single As dimer row, followed by the filling in of the adjacent trench sites, as seen in Fig. 6(b). From these local protrusions into the lower terrace, step-flow growth proceeds both by continuing growth along As dimer rows of the lower terrace and by extending the tails of these protrusions in the perpendicular directions, as seen in Figs. 6(c) and 6(d). The $\beta 2(2\times 4)$ structure is recovered when the wide As dimer rows split at the end of these protrusions. In these snapshots, the growth time varies between $t=0.5$ s in Fig. 6(a) and $t=2.0$ s in Fig. 6(d) with the fixed interval of $\Delta t=0.5$ s.

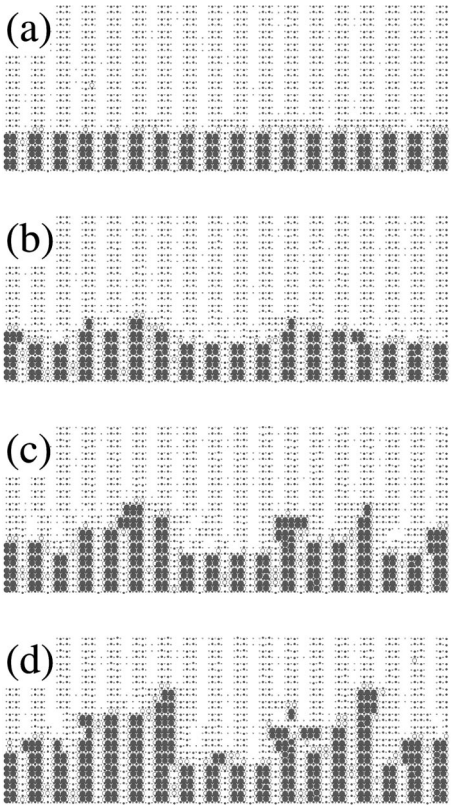

FIG. 6. A series of snapshots showing the simulated growth of the $B1$ terrace edge in Fig. 5(a). Ga and As_2 fluxes are 0.1 ML/s and 0.4 ML/s, respectively. The lattice size is $120a_s \times 120a_s$, and $g=5$ is used. (a) $t=0.5$ s. Ga adatoms reach the lower side of the terrace edge. (b) $t=1.0$ s. When single As dimer rows grow on top of the As dimer hills of the lower terrace, adjacent trenches are filled, and growth in the perpendicular direction also proceeds. (c) $t=1.5$ s. The As dimer rows at the ends of the protrusions become wide. (d) $t=2.0$ s. The wide As dimer rows split and the $\beta 2(2\times 4)$ structure is recovered.

Next, we simulate the growth of a $B2$ step. As Fig. 7(a) shows, Ga adatoms can easily reach the lower side of the terrace edge in the same manner as we saw in Fig. 6(a). However, in contrast to the growth of a $B1$ step, in order for the growth of a $B2$ step to proceed in the $[\bar{1}10]$ direction, the trench sites on the lower terrace must be filled in first and, hence, growth by the elongation of As dimer rows from the edge of the upper terrace becomes very inefficient. Accordingly, growth proceeds only in the directions perpendicular to As dimer rows via kink propagation, as seen in Figs. 7(b)–7(d). These snapshots were recorded with the same intervals of time as before.

The growth of a $B3$ step proceeds quite similarly to that of a $B1$ step, as seen in Figs. 8(a)–8(c). However, due to the phase difference in the $[\bar{1}10]$ direction between the upper terrace and the lower one, there appear many point defects, as we can see on the lower terrace by comparing Fig. 8(d) to Fig. 6(d). These defects obstruct the tails of the protruding

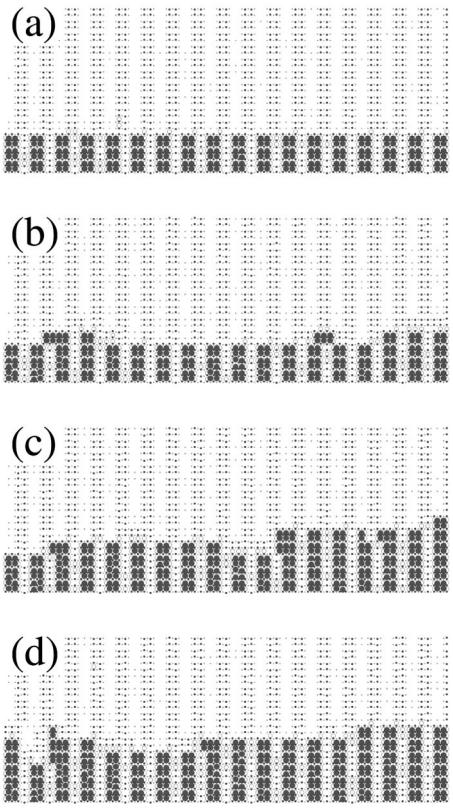

FIG. 7. A series of snapshots showing the simulated growth of the $B2$ terrace edge in Fig. 5(b). Ga and As_2 fluxes are 0.1 ML/s and 0.4 ML/s, respectively. The lattice size is $120a_s \times 120a_s$, and $g=3$ is used. Growth takes place by the propagation of kink structures in the direction perpendicular to the As dimer rows. (a) $t=0.5$ s. (b) $t=1.0$ s. (c) $t=1.5$ s. (d) $t=2.0$ s.

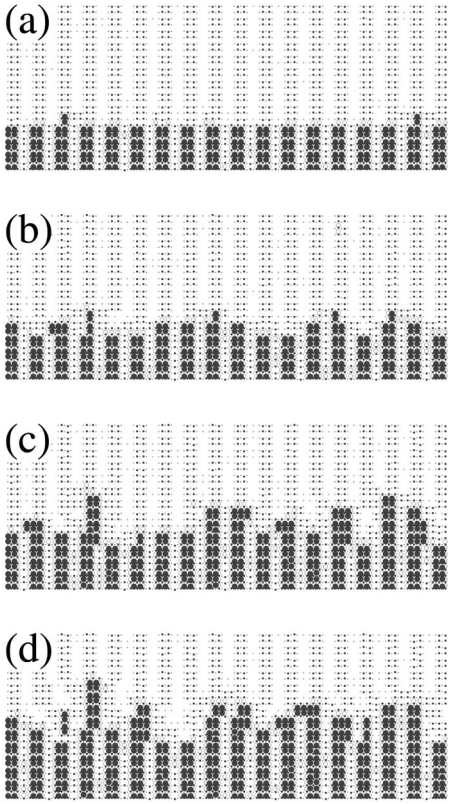

FIG. 8. A series of snapshots showing the simulated growth of the $B3$ terrace edge in Fig. 5(c). Ga and As_2 fluxes are 0.1 ML/s and 0.4 ML/s, respectively. The lattice size is $120a_s \times 120a_s$, and $g=3$ is used. The width of a growing As dimer row is restricted by the presence of surface defects caused by the phase shift in the $[\bar{1}10]$ direction. (a) $t=0.5$ s. (b) $t=1.0$ s. (c) $t=1.5$ s. (d) $t=2.0$ s.

peninsulas from extending over wide areas along the terrace edge, so that they do not become very wide. The intervals of the recorded growth times in Figs. 8(a)–8(d) are the same as those in Figs. 6(a)–6(d).

In contrast, the growth of a $B4$ step does not look so different from that of a $B2$ step, as seen in Figs. 9(a)–9(d). This is principally because dimer row growth in the $[\bar{1}10]$ direction scarely occurs in either case and, furthermore, the growth of a $B4$ step does not proceed entirely at a terrace edge unless point defects caused by the phase difference in the $[\bar{1}10]$ direction are filled in by deposited materials. Here, the time scale is twice as large as those in other snapshots, i.e., $t=1.0$ s in Fig. 6(a) and $t=4.0$ s in Fig. 6(d) with the interval of $\Delta t=1.0$ s.

Our results have shown that the effect of the phase differences for B steps is more prominent for a phase shift in the $[110]$ direction than in the $[\bar{1}10]$ direction. At the same time, they suggest that there is a difference in growth rate among these four kinds of B steps, i.e., the growth rate should decrease in the order from $B1$ to $B4$ via either $B2$ or $B3$. Although the snapshots in Figs. 6–9 do not clearly show this tendency, this is because islands are growing away from the terrace edges in all cases, so that the total amounts of deposited materials and the apparent growth rates are not linearly related with each other. Despite this, we can see this tendency in some of the snapshots at later stages of growth. For example, we can see in Fig. 10 that a $B4$ terrace edge, which is straight at first, has changed to a $B2$ terrace edge at each end, whereas it has changed to the $B1$ type in the central part. Obviously, these phenomena occurred because a $B4$ terrace edge is less efficient in growth than the $B1$ or $B2$ type.

III. COMPARISON WITH RHEED EXPERIMENTS

As we pointed out in Sec. I, the time evolution of specular RHEED intensity on an A surface, especially its behavior immediately after starting growth, cannot be accounted for by growth simulations based on the SOS model.[33] Therefore, we need to examine if this evolution can be reproduced by our simulations. To accomplish this task, it is necessary to increase the density of terrace edges so as to enhance its effect in the simulation results. To this aim, we use a configuration of two-level terraces of strips placed on a $120a_s \times 120a_s$ lattice, in which the lower and upper strips are given sizes of $80a_s \times 120a_s$ and $40a_s \times 120a_s$, respectively. With this configuration used as the initial condition, we carried out growth simulations by choosing $g=5$ and $g=1$, and obtained the time evolutions of the number densities of double

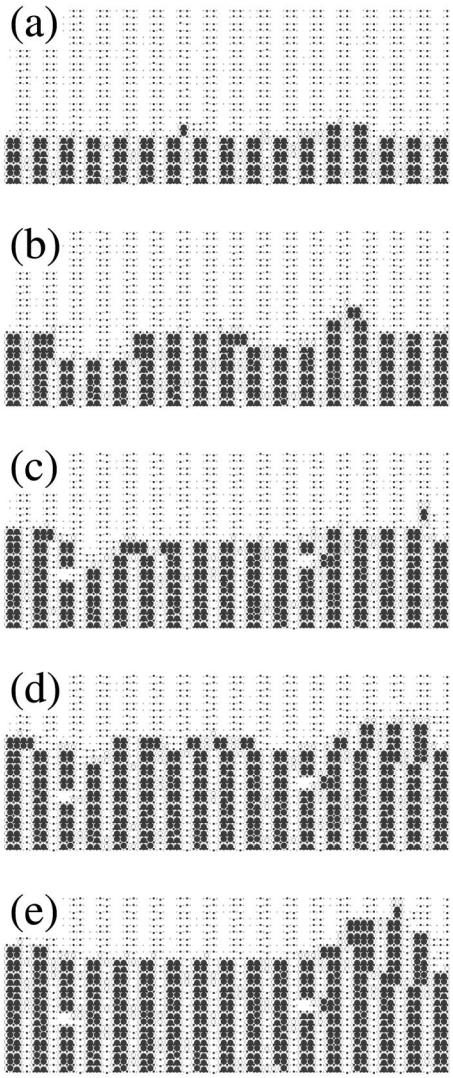

FIG. 9. A series of snapshots showing the simulated growth of the $B4$ terrace edge in Fig. 5(d). Ga and As_2 fluxes are 0.1 ML/s and 0.4 ML/s, respectively. The lattice size is $120a_s \times 120a_s$, and $g=3$ is used. Growth via kink propagation is enabled only when surface defects are filled in. (a) $t=1.0$ s. (b) $t=2.0$ s. (c) $t=3.0$ s. (d) $t=4.0$ s. (e) $t=5.0$ s.

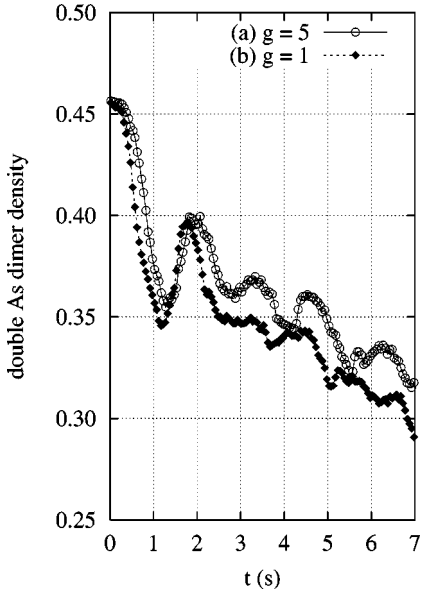

FIG. 11. Time evolutions of the densities of double As dimers obtained by simulations on a $120a_s \times 120a_s$ lattice, on which the first and second strips of $80a_s \times 120a_s$ and $40a_s \times 120a_s$ are stacked. Ga and As_2 fluxes are 0.1 ML/s and 0.4 ML/s, respectively. (a) $g=5$ and (b) $g=1$.

As dimers $\rho_{d\mathrm{As}}$, as this feature characterizes the $\beta 2(2\times 4)$ structure as well as the $\alpha(2\times 4)$ structure. Moreover, $\rho_{d\mathrm{As}}$ is found to evolve synchronously with the specular RHEED intensity on a singular GaAs(001) surface, as we reported previously,[11] so that it is important to examine if $\rho_{d\mathrm{As}}$ evolves synchronously with the specular RHEED intensity on an A surface also.

Figures 11(a) and 11(b) show the evolutions of $\rho_{d\mathrm{As}}$ for $g=5$ and $g=1$, respectively. As Fig. 11(a) shows, $\rho_{d\mathrm{As}}$ oscillates quickly when $g=5$ is used. This is because the stick-to-split growth mechanism repeats on an A surface, and an As dimer row at a terrace edge changes its width cyclically, as we saw in Fig. 4. In contrast, this oscillation becomes less prominent when $g=1$ is used, as seen in Fig. 11(b). On an A surface, generally the island growth mode is more likely than the step-flow growth mode for large values of g. With our particular configuration, however, a small value of g such as $g=1$ results in the nucleation of islands on top of the upper strip because Ga adatoms can migrate onto the top of it from both sides and may create an island when they collide with each other. In both cases, $\rho_{d\mathrm{As}}$ decreases rapidly after starting growth and reaches its first minimum at the coverage $\Theta_c \simeq 0.1$ ML, where the coverage Θ_c is defined by the product of Ga flux and growth time t. After reaching this minimum, $\rho_{d\mathrm{As}}$ increases quickly and reaches its first maximum at $\Theta_c \simeq 0.2$ ML. Similar features were observed in the specular RHEED intensities on A surfaces, as seen in Figs 1–3 of

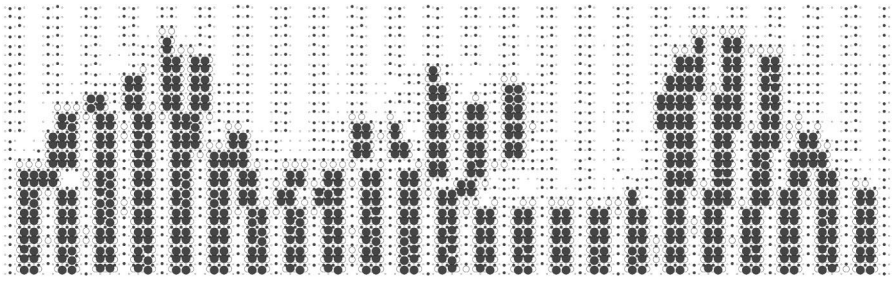

FIG. 10. A snapshot showing the transformation of a terrace edge from $B4$ to $B2$ at both ends and to $B1$ in the central part.

Ref. 33. However, on these real surfaces, g has a much larger value than those we used in our simulations, as we noted earlier. Because of this, nucleation and growth of islands are more enhanced on a real A surface than in our simulations. This is consistent with the fact that only one strong peak can be seen in Fig. 11(b) and in the specular RHEED intensities observed on A surfaces.[33]

IV. DISCUSSION

In Sec. II, we saw that, for an A step to grow, only a pair of Ga adatoms need be located by the lower side of a terrace edge so as to accommodate an As_2 molecule, whereas four of them are necessary for a B step to accomplish this task, as the shaded areas in Figs. 3(a) and 3(b) clearly show. Thus, from the viewpoint of Ga kinetics, step-flow growth on a B surface is not favored because the probability for a B step to acquire four Ga adatoms is certainly much smaller than that for an A step to capture only two of them. In our simulations, this disadvantage of growth in the $[\bar{1}10]$ direction is overcome by the strong fluctuation of the atomic structures on growing islands. More precisely, when Ga adatoms are not in the trench sites of the well-ordered $\beta 2(2\times 4)$ structure, the diffusion anisotropy of these atoms is enhanced in the direction perpendicular to an As dimer row,[8–10] so that there appears a strong fluctuation in island morphology, which results from the competition between this diffusion anisotropy of Ga adatoms and the Coulomb repulsion between surface As species acting principally in the $[110]$ direction. It is actually this fluctuation that enables an island to adopt the $\beta 2(2\times 4)$ structure rather quickly.[8–10] On a B surface with a straight step edge, however, this fluctuation is strongly suppressed, as we saw in Sec. II B. Therefore, partly because of this suppression of the fluctuation and partly because of the small probability of capturing four Ga adatoms, the growth of a straight B step is generally very inefficient compared with that of an island. Moreover, we have shown by the KMC simulations that the morphology of a growing B step depends strongly on the phase difference in the $\beta 2(2\times 4)$ structures between an upper terrace and a lower one. At the same time, the capture of Ga adatoms by an A step is inefficient, too, due to the diffusion anisotropy of Ga adatoms which is enhanced in the $[\bar{1}10]$ direction. Thus, a step-flow growth mode is generally a very inefficient process when it is compared to an island growth mode.

In Sec. II A, we saw that growth of an A step begins with the growth of rather short segments of As dimer rows. After a sufficiently long period of time, these segments sometimes merge into an As dimer row again, and the straight hill-and-trench structure of the $\beta 2(2\times 4)$ reconstruction is often recovered. However, this is not always the case, as seen in Figs. 4(j)–4(l), where we can find the remains of the short segments, which appeared to grow nearly independently of each other. Thus, our results showed that the growth of a straight A step proceeds, not in a coherent manner as was suggested by simulation studies based on the SOS model,[33] but by the splitting of rather short segments of an As dimer row. Recall that this phenomenon is caused principally by the diffusion anisotropy of Ga adatoms, which is usually enhanced in the direction parallel to the trenches of the $\beta 2(2\times 4)$ structure. Indeed, when Ga adatoms are allowed to diffuse isotropically, they can reach the terrace edges of an A surface much more easily, so that growth can proceed more smoothly by the occurrence of the stick-to-split growth mechanism in a rather coherent fashion. As is clear from our results, surface reconstruction, particularly its geometry, plays a crucial role in the growth of a semiconductor surface at an atomic scale, especially when the surface is in the step-flow growth mode. However, this important property cannot be taken into account in the one-species SOS model[33] or its simple two-species extension.[51–53] In particular, it is incorrect to attribute the anisotropic growth morphology of GaAs(001) to the sticking anisotropy of the diffusive species, because this is an artifact of the SOS model.[33,54]

Recently, we showed by the combined use of KMC simulations and *ab initio* calculations that the specular RHEED intensity on a GaAs(001)-$\beta 2(2\times 4)$ surface evolves synchronously with the density of double As dimers, and not with the step density, during growth and after its interruption.[11] We showed by our simulation results in Figs. 11(a) and 11(b) that the special features found in evolution of the specular RHEED intensities on A surfaces, as seen in Figs. 1–3 of Ref. 33, can be accounted for by the stick-to-split growth mechanism, due to which As dimer rows at an A step edge change their widths cyclically between 2 and 4, as seen in Fig. 4. This accounts for the clear difference in the initial stages of the evolution of the observed specular RHEED intensities between A surfaces and B or C surfaces at $T\simeq 580\,^{\circ}\mathrm{C}$.[33] To further achieve good agreement between simulations and specular RHEED intensities on an A surface, we must carefully take account of the possible change in the nucleation rate of islands on it due to the displacement of atomic structures associated with the change of width of an As dimer row at an A step edge.[11] Note that, even if this effect causes a considerable change in the morphology of a growing surface, it should be strictly distinguished from the Ehrlich-Schwoebel effect,[46–49] because the latter is not related to the local structural change of a surface reconstruction.

From RHEED observations, Shitara *et al.* noted a delay of the first maxima of specular RHEED intensities on vicinal surfaces.[33,55] They ascribed this phenomenon to the presence of ''incorporation barriers'' E_{I}, and obtained their values as 4.2 eV, 1.4 eV, and 2.1 eV, respectively, for the A, B, and C surfaces with the misorientation angle of $2\,^{\circ}$. In the model we used, the values of the largest and second largest barriers are $E_a=2.22$ eV and $E_b=1.88$ eV, which are associated with the desorption processes of the gray As dimers in Figs. 12(a) and 12(b), respectively. Compared with them, $E_{\mathrm{I}}^{A}=4.2$ eV (Refs. 33,55) seems too large. Therefore, it is quite possible that these delays are not caused by single-atomic or molecular kinetics, but by some composite kinetic processes that are not directly related to the incorporation of the deposited materials on an atomic step. This is also suggested by the strong dependence of the measured values of E_{I} on the growth conditions used.[56]

A recent STM observation revealed the presence of Ga clusters on the lower sides of the B steps.[57–60] The existence

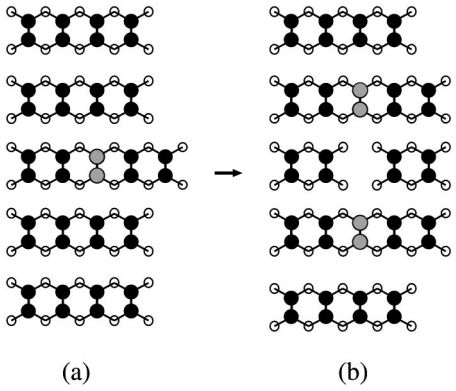

FIG. 12. (a) The desorption of an As dimer from the central site of the five-wide dimer row. The desorption barrier of the gray As dimer is 2.22 eV. (b) The splitting process that follows the desorption depicted in (a). The desorption barrier of each gray As dimer is 1.88 eV.

of these clusters indicates that a *B* step is inefficient at incorporating Ga adatoms for growth when compared with the rate of their diffusion. Therefore, taking proper account of the effect of these Ga clusters may enable us to determine the appropriate vicinal orientation for realizing a step-flow growth mode in MBE growth experiments. Indeed, comparison of our results with the STM images[57–60] suggests that if one uses an *A* surface a considerable number of Ga adatoms diffuse along the trenches of the $\beta 2(2\times4)$ structure without reaching a terrace edge, and eventually they may create islands when they collide with each other.[61] When a *B* surface is used, on the contrary, Ga adatoms reach a *B* step and make clusters at the lower side of it.[57,58] Moreover, the growth of straight *B* steps is found by our simulation studies to be unstable. This implies, therefore, that the appropriate vicinal orientation for stable step-flow growth mode is not the $[110]$ or $[\bar{1}10]$ direction. Rather, it may exist somewhere between them.

The shapes of the terrace edges we obtained by our growth simulations look very similar to the recently reported STM images.[57–60] We used growth conditions in which the substrate temperature is $T=580\,^{\circ}\mathrm{C}$, and the Ga and As_2 fluxes are 0.1 ML/s and 0.4 ML/s, respectively, i.e., the As_2-to-Ga flux ratio is 4. In these conditions, the *A* surface was found by RHEED observations to exhibit an island growth mode while the *B* surface has a step-flow growth mode.[33] By contrast, all of our simulations showed not only the growth of each terrace but also that of islands. In this sense, our results apparently disagree with the RHEED observations.

This discrepancy results partly from the fact that the angles of misorientation θ used in experiments are much larger than those used in our simulations. In fact, when a *B* surface of much smaller vicinal orientation is used, islands have been observed even after annealing.[61] At the same time, it may also partly result result from the fact that our model does not take account of the possible appearance of Ga clusters on the lower side of a *B* step. This is because the presence of such Ga clusters implies that the incorporation of Ga adatoms into a *B* step may not be an efficient process compared with their diffusion. Therefore, if this surplus of adatoms is consumed by making clusters, they can stay near a step edge, and may locally increase the effective chemical potential of Ga there, so that the growth rate of a *B* step may be increased. If this is not the case, on the contrary, they will diffuse away from there and make islands somewhere else because, according to our simulations, this process is more efficient than step-flow growth. The former may occur on a real surface, on which the latter can also take place if the terrace width is very large, but only the latter can occur in our simulations, in which no effects related to the existence of Ga clusters are taken into account. In order to have a quantitative estimate of the role of Ga clusters in the growth of a *B* surface, we need to know the binding energy of a Ga atom to a cluster, and also its dependency on the cluster size. This may be accomplished by *ab initio* density functional or empirical molecular dynamics calculations.

Finally, we mention the presence of a discrepancy between our model and the results of *ab initio* density functional calculations. To determine the parameters of the model, quantitative comparisons were made of the morphology of growing 2D islands between simulations and the STM images,[8–10,45] as we mentioned in Sec. II. In this process, the precise site dependence of the binding energy of a Ga adatom was not considered, yet very good agreement was obtained in comparison of the island size distributions between simulations and experiments in the precoalescence regime, i.e., at $\Theta_c<0.2$ ML.[9,10] However, *ab initio* density functional calculations have revealed that the binding energy of a Ga adatom does depend on whether it is bonded onto the atop site of an As dimer pair or onto the interdimer site.[7,34] This implies that the empirical parameters we used in our simulations may correspond to the approximate values obtained by taking averages over such distinct sites.[63–66] Indeed, there is even criticism of the use of empirical parameters to carry out KMC simulations.[62] However, the facts that we could obtain good agreement in the island size distributions between simulations and experiments[9,10] and also that we could identify the origin of the evolution of the specular RHEED intensity on a growing GaAs(001)-$\beta 2(2\times4)$ surface and in the recovery process after its interruption[11] indicate that the evolution of surface morphology is rather insensitive to such precise site dependence of the binding energies of the Ga adatom. Instead, our results suggest that the molecular and surface dimer kinetics of As species are much more important. However, further studies are needed, in both theory and experiment, to examine if our simulations are good approximations for step-flow growth too, or whether the surface morphology is significantly altered when the precise site dependence of the binding energies of the Ga adatom is taken into account.

V. CONCLUSION

We have used a two-species kinetic growth model of the GaAs(001)-$\beta 2(2\times4)$ reconstruction to study step-flow growth modes of *A* and *B* steps at an atomic scale. We revealed that growth of an *A* step proceeds by creating rather

short segments of As dimer rows due to the diffusion anisotropy of Ga adatoms. Although these segments are usually found to merge later, this does not mean that the growth of an *A* step proceeds coherently over a long distance along an As dimer row. On a *B* step, we found that the phase difference of the $\beta 2(2\times4)$ structure between an upper terrace and a lower one plays a crucial role in determining the morphology of the growing terrace edge. When two terraces are in phase with each other in the $[110]$ direction, an As dimer row grows on top of an As dimer row of the lower terrace, followed by the growth of this As dimer row in the directions perpendicular to it, and consequently there appears a peninsula consisting of the $\beta 2(2\times4)$ structure. On the contrary, if the two terraces are out of phase with each other in the $[110]$ direction, growth proceeds via kink propagation in the direction perpendicular to the As dimer rows. In contrast to these two cases, the phase difference between two terraces in the $[\bar{1}10]$ direction results in the appearance of many surface defects. Since this is disadvantageous, we found that such terraces usually transform into in-phase terraces during growth.

Our results showed that growth does not proceed at *A* or *B* steps efficiently or coherently. This suggests that the appropriate vicinal orientation for a stable step-flow growth mode exists in a direction somewhere between $[\bar{1}10]$ and $[110]$.

Finally, the simulated growth of the *A* steps was compared with the results of specular RHEED intensity observations, to find qualitative agreement.

ACKNOWLEDGMENTS

The authors are grateful to J. H. Neave, T. Kaneko, Y. Asaoka, H. Mihara, and S. Tsukamoto for fruitful discussions, and to G. R. Bell for showing us his STM images before publication. One of the authors (M.I.) thanks Y. Akutsu, M. P. Blencowe, M. Chu, and E. Hofstetter for their encouragement.

*Present address: Department of Physics, Graduate School of Science, Osaka University, Toyonaka, Osaka 560-0043 Japan. Electronic address: makoto@acty.phys.sci.osaka-u.ac.jp

[1] T. Ito and K. Shiraishi, Surf. Sci. **37-38**, 486 (1996).
[2] T. Ito and K. Shiraishi, Jpn. J. Appl. Phys., Part 2 **35**, L949 (1996).
[3] K. Shiraishi and T. Ito, Phys. Rev. B **57**, 6301 (1998).
[4] T. Ito and K. Shiraishi, Jpn. J. Appl. Phys., Part 2 **35**, L1016 (1996).
[5] T. Ito and K. Shiraishi, Jpn. J. Appl. Phys., Part 2 **37**, L262 (1998).
[6] C.G. Morgan, P. Kratzer, and M. Scheffler, Phys. Rev. Lett. **82**, 4886 (1999).
[7] P. Kratzer, C.G. Morgan, and M. Scheffler, Phys. Rev. B **59**, 15 246 (1999).
[8] M. Itoh, G.R. Bell, A.R. Avery, T.S. Jones, B.A. Joyce, and D.D. Vvedensky, Phys. Rev. Lett. **81**, 633 (1998).
[9] M. Itoh, Ph.D. thesis, University of London, 1999. The minor revised version is available at http://wwwacty.phys.sci.osaka-u.ac.jp/~makoto/
[10] M. Itoh, G.R. Bell, B.A. Joyce, and D.D. Vvedensky, Prog. Theor. Phys. Suppl. **138**, 90 (2000).
[11] M. Itoh and T. Ohno, Phys. Rev. B **62**, 7219 (2000).
[12] M. Itoh and T. Ohno, Phys. Rev. B **62**, 1889 (2000).
[13] K. Tanahashi, Y. Kawamura, N. Inoue, Y. Homma, and J. Osaka, J. Cryst. Growth **188**, 205 (1998).
[14] W. Barvosa-Carter, A.S. Bracker, J.C. Culbertson, B.Z. Nosho, B.V. Shanabrook, L.J. Whitman, H. Kim, N.A. Modine, and E. Kaxiras, Phys. Rev. Lett. **84**, 4649 (2000).
[15] H. Chen, R.M. Feenstra, J.E. Northrup, T. Zywietz, and J. Neugebauer, Phys. Rev. Lett. **85**, 1902 (2000).
[16] J.E. Northrup and J. Neugebauer, Phys. Rev. B **60**, R8473 (1999).
[17] J.E. Northrup, J. Neugebauer, and L.T. Romano, Appl. Phys. Lett. **74**, 2319 (1999).
[18] A.R. Smith, R.M. Feenstra, D.W. Greve, J. Neugebauer, and J.E. Northrup, Phys. Rev. Lett. **79**, 3934 (1997).
[19] Q.-K. Xue, Q.Z. Xue, R.Z. Bakhtizin, Y. Hasegawa, I.S. Tsong, T. Sakurai, and T. Ohno, Phys. Rev. Lett. **82**, 3074 (1999).
[20] S.-H. Lee, W. Moritz, and M. Scheffler, Phys. Rev. Lett. **85**, 3890 (2000).
[21] W.G. Schmidt, S. Mirbt, and F. Bechstedt, Phys. Rev. B **62**, 8087 (2000).
[22] C. Ratsch, W. Barvosa-Carter, F. Grosse, J.H. Owen, and J.J. Zinck, Phys. Rev. B **62**, R7719 (2000).
[23] For reviews on the GaAs(001)-(2×4) structures, see C.M. Goringe, L.J. Clark, M.H. Lee, M.C. Payne, I. Štich, J.A. White, M.J. Gillan, and A.P. Sutton, J. Phys. Chem. **101**, 1498 (1997); Q.-K. Xue, T. Hashizume, and T. Sakurai, Prog. Surf. Sci. **56**, 1 (1997).
[24] *Molecular Beam Epitaxy*, edited by Alfred Cho (AIP Press, Woodbury, NY, 1994).
[25] J.J. Harris, B.A. Joyce, and P.J. Dobson, Surf. Sci. **103**, L90 (1981).
[26] W. Braun, *Applied RHEED* (Springer-Verlag, Berlin, 1999).
[27] J.H. Neave, P.J. Dobson, B.A. Joyce, and J. Zhang, Appl. Phys. Lett. **47**, 100 (1985).
[28] A.B. Bortz, M.H. Kalos, and J.L. Lebowitz, J. Comput. Phys. **17**, 10 (1975).
[29] P.A. Maksym, Semicond. Sci. Technol. **3**, 594 (1988).
[30] M. E. J. Newman and G. T. Barkema, *Monte Carlo Methods in Statistical Physics* (Oxford University Press, Oxford, 1999).
[31] T. Shitara, D.D. Vvedensky, M.R. Wilby, J. Zhang, J.H. Neave, and B.A. Joyce, Appl. Phys. Lett. **60**, 1504 (1992).
[32] T. Shitara, D.D. Vvedensky, M.R. Wilby, J. Zhang, J.H. Neave, and B.A. Joyce, Phys. Rev. B **46**, 6815 (1992).
[33] T. Shitara, D.D. Vvedensky, M.R. Wilby, J. Zhang, J.H. Neave, and B.A. Joyce, Phys. Rev. B **46**, 6825 (1992).
[34] A. Kley, P. Ruggerone, and M. Scheffler, Phys. Rev. Lett. **79**, 5278 (1997).
[35] A. Bogicevic, J. Strömquist, and B.I. Lundqvist, Phys. Rev. Lett. **81**, 637 (1998).
[36] S. Ovesson, A. Bogicevic, and B.I. Lundqvist, Phys. Rev. Lett. **83**, 2608 (1999).
[37] T.-Y. Fu and T.T. Tsong, Phys. Rev. B **61**, 4511 (1999).
[38] U. Köhler, C. Jensen, A.C. Schindler, L. Brendel, and D.E. Wolf, Philos. Mag. B **80**, 283 (2000).

[39] U. Köhler, C. Jensen, C. Wolf, A.C. Schindler, L. Brendel, and D.E. Wolf, Surf. Sci. **454-456**, 676 (2000).
[40] C.T. Foxon and B.A. Joyce, Surf. Sci. **50**, 434 (1975).
[41] C.T. Foxon and B.A. Joyce, Surf. Sci. **64**, 293 (1977).
[42] E.S. Tok, J.H. Neave, J. Zhang, B.A. Joyce, and T.S. Jones, Surf. Sci. **374**, 397 (1997).
[43] E.S. Tok, T.S. Jones, J.H. Neave, J. Zhang, and B.A. Joyce, Appl. Phys. Lett. **71**, 3276 (1997).
[44] The correct interaction diagrams of the Ga part of the model can be seen in Refs. 9 and 10 but not in Ref. 8.
[45] G.R. Bell, T.S. Jones, M. Itoh, and B.A. Joyce, Surf. Sci. **423**, L280 (1999).
[46] G. Ehrlich and F.G. Hudda, J. Chem. Phys. **44**, 1039 (1966).
[47] R.L. Schwoebel, J. Appl. Phys. **40**, 614 (1968).
[48] A. Pimpinelli and J. Villain, *Physics of Crystal Growth* (Cambridge University Press, Cambridge, 1998).
[49] A.-L. Barabási and H. E. Stanley, *Fractal Concepts in Surface Growth* (Cambridge University Press, Cambridge, 1995).
[50] J.E. Northrup and S. Froyen, Phys. Rev. B **50**, 2015 (1994).
[51] A. Ishii and T. Kawamura, Appl. Surf. Sci. **130-132**, 403 (1998).
[52] A. Ishii and T. Kawamura, Surf. Sci. **436**, 38 (1999).
[53] T. Kawamura and A. Ishii, Surf. Sci. **438**, 155 (1999).
[54] V.P. LaBella, D.W. Bullock, Z. Ding, C. Emery, W.G. Harter, and P.M. Thibado, J. Vac. Sci. Technol. A **18**, 1526 (2000).
[55] T. Shitara, J. Zhang, J.H. Neave, and B.A. Joyce, J. Appl. Phys. **71**, 4299 (1992).
[56] T. Kaneko (private communication).
[57] A.R. Avery, D.M. Holmes, T.S. Jones, B.A. Joyce, and G.A.D. Briggs, Phys. Rev. B **50**, 8098 (1994).
[58] S. Tsukamoto and N. Koguchi, J. Cryst. Growth **201/202**, 118 (1998).
[59] G.R. Bell, T.S. Jones, and B.A. Joyce, Surf. Sci. **429**, L492 (1999).
[60] G.R. Bell, T.S. Jones, J.H. Neave, and B.A. Joyce, Surf. Sci. **458**, 247 (2000).
[61] C.W. Snyder, J. Sudijono, C.-H. Lam, D.J. Johnson, and B.G. Orr, Phys. Rev. B **50**, 18 194 (1994).
[62] M. Scheffler, P. Kratzer, and L. G. Wang, in *Proceedings of the 4th Symposium on Atom-Scale Surface and Interface Dynamics, 2000, Tsukuba, Japan*, edited by A. Oshiyama (Japan Society for the Promotion of Science), pp. 3–7; http://www.fhi-berlin.mpg.de/th/pub00.html
[63] I. Vattulainen, J. Merikoski, T. Ala-Nissila, and S.C. Ying, Phys. Rev. Lett. **79**, 257 (1997).
[64] I. Vattulainen, J. Merikoski, T. Ala-Nissila, and S.C. Ying, Phys. Rev. B **59**, 7697 (1999).
[65] I. Vattulainen, J. Merikoski, T. Ala-Nissila, and S.C. Ying, Phys. Rev. B **57**, 1896 (1998).
[66] S.C. Ying, I. Vattulainen, J. Merikoski, T. Hjelt, and T. Ala-Nissila, Phys. Rev. B **58**, 2170 (1998).